Physics and Imaging in Radiation Oncology 34 (2025) 100762

Contents lists available at ScienceDirect

Physics and Imaging in Radiation Oncology

journal homepage: www.sciencedirect.com/journal/physics-and-imaging-in-radiation-oncology

Technical Note

A 0.05 mm^3 diode-based single charged-particle real-time radiation detector for electron radiotherapy

Kyoungtae Lee [a,b,*], Rahul Lall [c], Michel M. Maharbiz [c], Mekhail Anwar [a,c,**]

[a] The University of California, San Francisco, USA
[b] Daegu Gyeongbuk Institute of Science and Technology (DGIST), South Korea
[c] The University of California, Berkeley, USA

ARTICLE INFO

Keywords:
Single-particle sensitive dosimetry
Electron EBRT
Integrated circuit based dosimeter

ABSTRACT

Real-time radiation monitoring at the single-particle level is an unmet need for electron radiotherapy, especially for dose deposition to targets in motion or critical OARs. We have developed a first-in-class CMOS-based 0.05 mm^3 single electron sensitive detector. The chiplet integrates all the requisite electronics. The functionality of the system is verified under 6 and 9 MeV clinical electron beams. Percentage depth vs. pulse-width curves for 6 and 9 MeV beams are measured and verified using Monte-Carlo simulations. The proposed system has the potential to enhance the electron radiotherapy quality and safety, providing real-time dosimetry from multiple sites simultaneously.

1. Introduction

Delivering the optimal dose of radiation to the tumor while minimizing unwanted energy deposition in the surrounding organs at risk (OAR) is a critical challenge for radiotherapy quality and safety in the modern era of dose escalation, combination systemic therapies, and tumor (and OAR) motion. To date, there is an unmet need to quantify electron dose in real-time for applications not only in clinics, such as intraoperative radiotherapy, superficial skin treatments, and electron boosts, but also in research, including cell culture or animal irradiation experiments [1].

Despite advances in radiation modeling and real-time image guided radiotherapy, state-of-the-art electron EBRT continues to suffer from a lack of ground-truth knowledge of the biological damage to the tumor and surrounding OARs. Radiation dose is the total energy deposition, $\sum E_{dep}$, per unit mass. However, the dose only reflects the cumulative E_{dep}, neglecting the nonlinear relationship between linear energy transfer (LET) and biological damage (i.e., the number of double strand breaks in DNA) at a single-particle level [2,3]. For example, 1,000 electrons depositing 1 keV each have the same total energy deposition as a single electron depositing 1 MeV, but they have significantly different biological effects due to differences in the LET. Although electrons have relatively flat LET values (±5 % variation in water) from 0.5 to 6 MeV, LET rapidly increases by ten times as the electron energy approaches 0 MeV. As a result, in a percentage depth-dose curve for a 6 MeV electron beam, dose to the target from 0 to 30 mm is mainly due to the electron flux, but variation in the LET more significantly affects the dose after 30 mm. This becomes critical as the fall-off of electrons may be placed just anterior to a critical structure, with the intention of sparing this structure. However, even a small number of electrons with high LET at the end range can be detrimental to the OAR. Especially near heterogenous anatomy, it becomes increasingly important to accurately quantify both the electron flux and LET, and not solely relying on total energy deposited. Therefore, the next generation dosimeter needs to have single-particle sensitivity to allow for an accurate record of scattered particles, and to enable the detection of the mismatch between predicted dose and delivered dose in real-time. This further allows for a safe dose escalation strategy. For example, a harmless ultra-low dose rate test beam can be applied first, and then the beam parameters can be adjusted based on the sensor reading to ensure the desired LET delivery to the tumors and OARs is achieved during the actual treatment.

Here, we present the world's first diode-based single electron sensitive sub-mm^3 radiation detector with integrated read-out circuitry, capable of real-time dosimetry for charged particles at the single-particle level. By exploiting CMOS fabrication technology, 4,096 ultra-small (1 μm^2) sensors with in-pixel analog and digital circuits for signal

* Corresponding author at: E3-512 DGIST, 333 Techno Jungang Daero, Hyeonpung-Eup, Daegu 42988, South Korea.
** Corresponding author at: 1825 Fourth St., First Floor, Room L1101, San Francisco, CA 94158, USA.
E-mail addresses: kyoungtae@dgist.ac.kr (K. Lee), Mekhail.Anwar@ucsf.edu (M. Anwar).

https://doi.org/10.1016/j.phro.2025.100762
Received 25 October 2024; Received in revised form 26 March 2025; Accepted 26 March 2025
Available online 2 April 2025

amplification and readout are integrated in a monolithic silicon chiplet (0.05 mm^3) [4]. The sensor monitors and relays the electron flux and LET information in real-time with the form factor and power consumption (<600 μW) compatible with future wireless implantation. The functionality of the system is verified under clinical 6 and 9 MeV electron beams using Siemens ONCOR linear accelerator.

2. Materials and methods

2.1. System design

The chip consists of a 64 × 64 diode array with in-pixel analog circuitry for signal amplification and a digital block that conveys the measured signal off-chip. In the pixel, P-N diodes detect electrons interacting with the silicon (see Fig. 1(a)). About a third of the energy deposited in the depletion region creates electron-hole pairs (EHPs), which are then integrated on a nearby capacitor (C_{int} = 3 fF), creating a voltage pulse (V_p) [5]. V_p is inversely proportional to the parasitic capacitance, and a nearly minimum size diode (1 μm^2) maximizes the signal from a single-particle hit. Instead of directly sampling V_p in the voltage domain, we measure the time for V_p to go back to its baseline (i.e., pulse width, PW), converting the signal to the time domain. The PW is monotonic and logarithmic to E_{dep} as shown below.

$$PW = \tau \times \frac{q \times qu \times E_{dep}}{E_g \times V_{trigger} \times C_{int}} = \tau \ln(\alpha E_{dep}) \quad (1)$$

where τ is the time constant at the diode node, q is the electron charge, qu is the quenching effect ratio ($\sim 1/3$), E_g is the silicon bandgap energy (1.12 eV), and $V_{trigger}$ is the minimum V_p that triggers the output. In this work, measured sum of PW, $\sum_{i=1}^{N} PW_i = \tau \sum_{i=1}^{N} \ln(\alpha E_{dep,i})$, is compared with the dose, $\sum_{i=1}^{N} E_{dep,i}$, from Monte-carlo simulation.

To have a large enough detection area, diodes are arranged in a 64 × 64 array. Each pixel contains its own amplifying circuit (see Fig. 1(b)), resulting in a total detection area of 512 × 512 μm^2 with a fill factor of 1/64. The data processing consists of an addressing block, data buffer, and clock generation circuitry. The generated digital pulses are stored and streamed off-chip. The chip is fabricated using a 65 nm CMOS technology. The overall size of the chip is 0.94 × 0.96 × 0.05 mm^3. Note that unlike conventional dosimeters, a silicon dioxide layer of only 10 μm covers the sensor, minimizing electron energy loss before reaching the detector.

2.2. Experimental setup

Fig. 1(d) and (e) show the experimental setup diagram and photo, respectively. Using a linear accelerator, the device is irradiated under clinical 6 and 9 MeV electron beams. A 10 × 10 cm^2 applicator with a 5.4 cm diameter Cerrobend collimator is used. Water-equivalent plastics (Plastic Water, CIRS) are used to mimic the water. The surface of the plastic water is placed at the isocenter. To quantify the uncertainty of each measurement, a leave-one-out Jackknife estimate (n = 30) of the standard error method is used [6]. The sensor outputs PW information of each single electron hit. At each water depth, measured count (number of single electron hits), mean PW (average PW of electron hits), and sum of PW (summation of all PWs) are acquired. Note that PW reflects LET; higher LET gives higher PW. In addition, to test the angular dependency

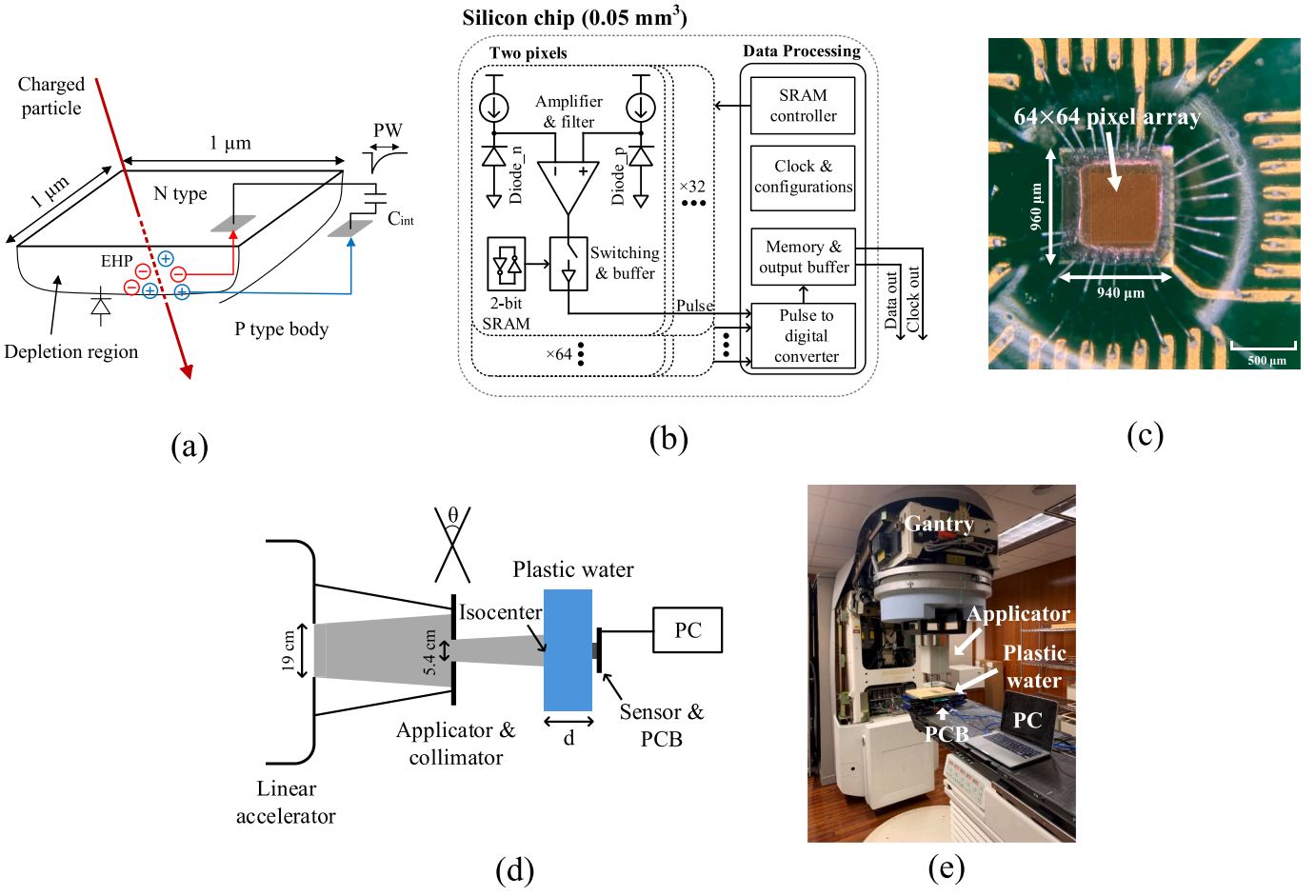

Fig. 1. (a) Diode-based detection mechanism. (b) System diagram of 64 × 64 single electron detector. (c) Chip photo. (d) Experimental setup diagram. (e) Experimental setup photo.

of the sensor, the angle of the incident beam is varied from 0° to 80°, with respect to the axis perpendicular to the device, under a 6 MeV electron beam at d = 0 and 14 mm. The sensor is placed at the isocenter at every angle.

2.3. TOPAS simulation setup

GEANT4-based Monte-Carlo simulator, the Tool for Particle Simulation (TOPAS), is used to verify the measurement results [7,8]. The sensor is modeled as a silicon box that is 0.1 × 0.1 × 0.04 mm^3 (0–30

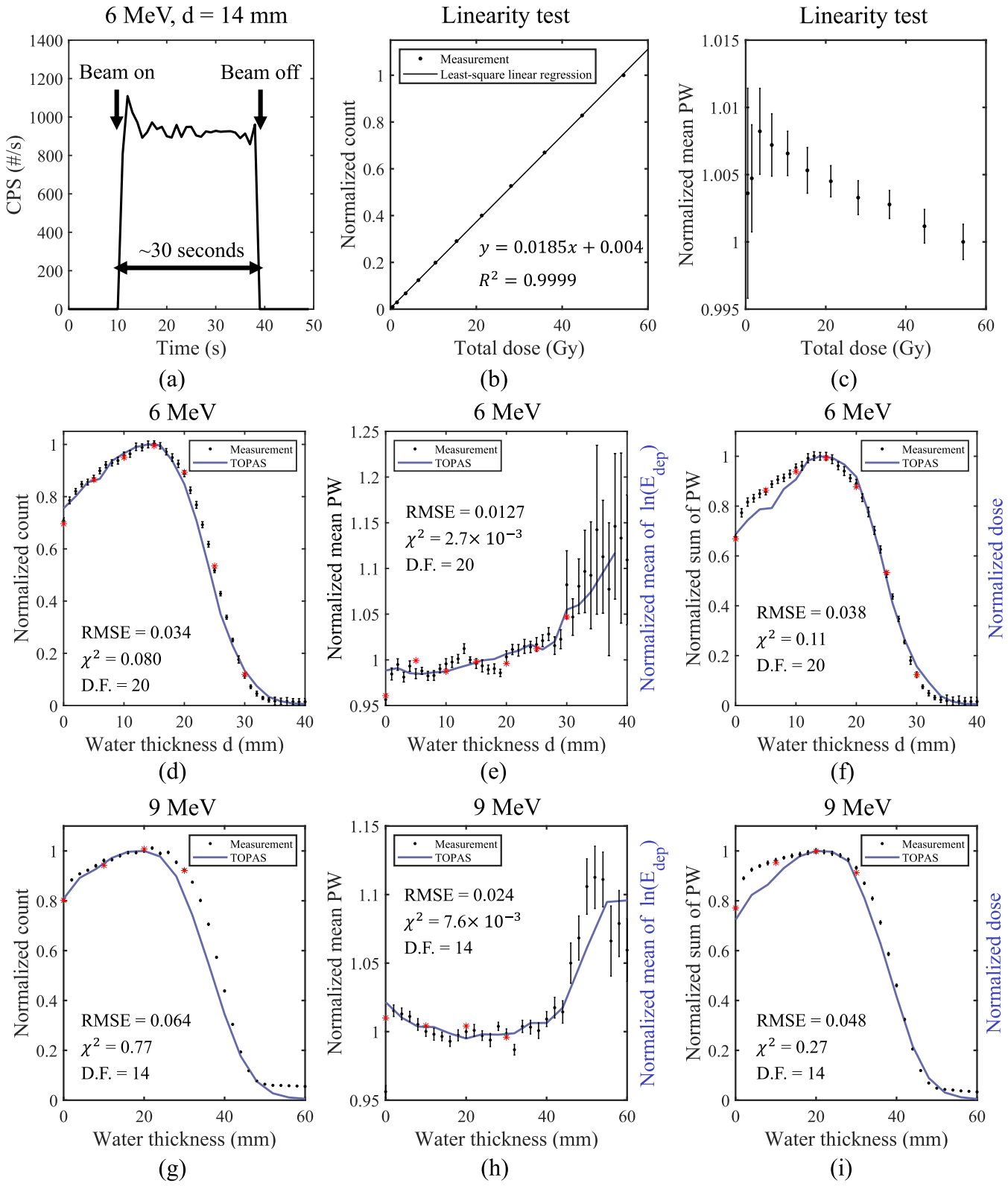

Fig. 2. Measured results of (a) transient counts per second (CPS) versus time; (b)-(c) linearity test, normalized at 55 Gy. Measured and TOPAS simulated results of (d)-(f) 6 MeV, normalized at d = 14 mm; (g)-(i) 9 MeV, normalized at d = 20 mm. In (e) and (h), the simulated E_{dep} is plotted and compared to the mean PW.

mm and 0–40 mm water depth for 6 and 9 MeV beam, respectively) and $0.5 \times 0.5 \times 0.2$ mm^3 (after 30 mm and 40 mm water depth for 6 and 9 MeV beam, respectively) due to the extensive simulation time of TOPAS. More detailed simulation parameters and geometry information are provided in the Supplementary Information (See Table. S1).

3. Results

At 0 Gy/min, the measured flux (number of electron hits per second) is zero. When the beam is turned on with the dose rate of ~ 1.5 Gy/min, the measured flux immediately surges and stabilizes at $6.62 \times 10^5 \pm 1.94 \times 10^4$ hits/mm^2/s (at a water depth of 14 mm) and $6.43 \times 10^5 \pm 4.59 \times 10^4$ hits/mm^2/s (at a water depth of 20 mm) for 6 and 9 MeV electron beams, respectively. The duration of the measured flux on chip corresponds exactly to the duration that the beam is on (See Fig. 2(a)). The overall response time is about 50 ms.

To test the linearity, the device is irradiated a total of 55 Gy under a 6 MeV electron beam at d = 0 mm. As shown in Fig. 2(b), the measured flux is linearly proportional to the total dose delivered. R^2 value from the least square linear regression is 0.9999, showing a highly linear relationship. In Fig. 2(c), the mean PW is relatively constant over the entire dose. A slight decline in PW (less than 1 % over 60 Gy) represents sensor degradation with radiation. However, this variation is within acceptable limits.

Fig. 2(d)–(i) shows the depth-PW curves for 6 MeV and 9 MeV beams. Build-up region, peak, fall-off region, and Bremsstrahlung tail are all apparent in the depth-PW curves. After the initial sweep through water thickness, a few water thicknesses are selected for repeat measurements to assess for any device degradation from radiation (shown as red asterisks). The data from the repeat measurements matches well with that from the initial sweep.

In Fig. 2(e) and (h), the TOPAS simulated mean of $\ln(E_{dep})$ is shown in blue, as the sensor detects the PW which is proportional to $\ln(E_{dep})$ (see Eq. (1)). The root mean square error (RMSE) values at 6 MeV and 9 MeV are 0.013 and 0.0053, respectively, demonstrating a good agreement between the measurement and simulation. Given that the measured count matches well with the simulated result at all water thicknesses, the deviation of the measured sum of PW and simulated dose is due to the logarithmic relationship between the E_{dep} and PW. Note that in both simulation and measurement for 6 and 9 MeV beam, mean PW and $\ln(E_{dep})$ after R_{90} is much higher (see Fig. 2(e) and (h)), indicating that the biological effect after R_{90} cannot be solely determined by the dose value. Finally, the comparison of clinically relevant parameters between the measurement and simulation is summarized in Table. S2. All the measured parameters are within 5 % of the simulated.

4. Discussion

The 64 × 64 diode-based single electron detector is proposed and tested under clinical beam settings. Measurement results and comparison with TOPAS under a clinical 6 MeV and 9 MeV electron beam show that the proposed system can measure single electrons with low uncertainty. This was possible due to the diode-based approach, which provides real-time voltage pulse proportional to the E_{dep} at the single-particle level.

The next generation *in vivo* dosimetry needs be sensitive enough to provide single-particle information (number of particles and LET of each) to accurately analyze the true biological effect by the radiation. A given dose can be due to either a large number of particles with low LET or few particles with high LET, but they have different biological damage. For example, the single-particle sensitivity would improve our clinical understanding near the Bremsstrahlung tail, as the dose deposition is mainly by a small number of high LET electrons. As a result, the proposed system may be used to evaluate the higher density of DNA damage near R_{90}, often referred to as the end-of-range effect. Thus, it is worth noting that the sensor readout (i.e., the normalized sum of PWs) is related to the relative biological effectiveness (RBE)-weighted dose. Also, the proposed system can enhance the treatment efficacy especially when the target is surrounded by complex anatomical structures (e.g., bones and air cavities) which are not trivial to model and simulate.

Despite many types of dosimeters that have been proposed for dose assessment during electron EBRT, none of them measures real-time single-particle information. Film dosimeters have been most widely used to measure the entry dose on patient's skin due to low cost and high spatial resolution. However, it lacks single-particle sensitivity and requires processing time [9]. Although metal-oxide-silicon field-effect-transistors (MOSFET) type dosimeters have the advantages of simple read-out circuitry, ease of fabrication, and low cost, they measure the accumulated dose deposited in the SiO_2 layer and lack the single-particle sensitivity [10,11]. Plastic scintillator, thermo-luminescence, and optically-stimulated luminescence dosimeters measure photons generated in the materials [12–14], requiring external, bulky, and power-hungry optical read-out circuitry, precluding real-time readout in a monolithic platform.

To enable the proposed system to be used in clinical settings, several technical challenges must be addressed. First, wireless power transfer and data transmission are required for implantation in the patient. Because of the system's low power consumption (~0.6 mW) and data rate (~4 kBps), RF or ultrasonic based methods are all well applicable [15,16]. An antenna, power management circuit, and modulator/demodulators are the only requisite components, occupying a small form factor (<1 mm^3). Next, the system needs a biocompatible coating. A thin (~50 μm) layer of Parylene or ceramic packaging can prevent device degradation due to biofluid penetration for more than 6 months, sufficient to cover the whole treatment cycle [17,18].

CRediT authorship contribution statement

Kyoungtae Lee: Conceptualization, Methodology, Software, Validation, Formal analysis, Writing – original draft, Visualization. **Rahul Lall:** Validation, Writing – original draft. **Michel M. Maharbiz:** Writing – original draft, Supervision, Funding acquisition. **Mekhail Anwar:** Conceptualization, Writing – original draft, Supervision, Project administration, Funding acquisition.

Declaration of competing interest

The authors declare the following financial interests/personal relationships which may be considered as potential competing interests: M.M.M. is a co-CEO of iota Biosciences, Inc, a subsidiary of Astellas Pharma (no overlap in business interests or projects). M.M.M. and M.A. have a patent (US201662359672P) related to in vivo radiation sensing. No other potential conflicts of interest relevant to this article exist.

Acknowledgement

This work was supported by the National Research Foundation of Korea (NRF) grant funded by the Korea government (MSIT) (RS-2024-00347277 and RS-2024-00419286).

A Funding Statement

This work is supported by the following sources.

1. University of California, San Francisco Resource Allocation Program (RAP) cancer center - cancer center support grant (CC-CCSG)
2. The Department of Defense Idea Development Award (PC220421)
3. National Research Foundation of Korea (NRF), South Korea (No. RS-2024-00347277)
4. National Research Foundation of Korea (NRF), South Korea (No. RS-2024-00419286)

Appendix A. Supplementary data

Supplementary data to this article can be found online at https://doi.org/10.1016/j.phro.2025.100762.

References

[1] Hogstrom KR, Almond PR. Review of electron beam therapy physics. Phys Med Biol 2006;51:455–89.
[2] Goodhead DT, Munson RJ, Thacker J, Cox R. Mutation and inactivation of cultured mammalian cells exposed to beams of accelerated heavy ions IV. biophysical interpretation. Int J Radiat Biol Re 1980;37:135–67.
[3] Goodhead DT. Initial events in the cellular effects of ionizing radiations: clustered damage in DNA. Int J Radiat Biol 1994;65:7–17.
[4] Lee K, Scholey J, Norman EB, Daftari IK, Mishra KK, Faddegon BA, et al. A millimeter-scale single charged particle dosimeter for cancer radiotherapy. IEEE J Solid State Circuits 2020;55:2947–58.
[5] Alig RC, Bloom S. Electron-hole-pair creation energies in semiconductors. Phys Rev Lett 1975;35:1522–5.
[6] Efron B. Chapter 3, The Jackknife, the Bootstrap and Other Resampling Plans. CBMS-NSF Regional Conference Series in Applied Mathematics, SIAM 1982.
[7] TOPAS: Tool for particle simulation. Accessed: July. 2024. [Online] Available: http://topasmc.org.
[8] Perl J, Shin J, Schumann J, Faddegon B, Paganetti H. TOPAS: An innovative proton Monte Carlo platform for research and clinical applications. Med Phys 2012;39:6818–37.
[9] Van Battum LJ, Huizenga H. Film dosimetry of clinical electron beams. Int J Radiat Oncol Biol Phys 1990;18:69–76.
[10] Beyer GP, Mann GG, Pursley JA, Espenhahn ET, Fraisse C, Godfrey DJ, et al. An implantable MOSFET dosimeter for the measurement of radiation dose in tissue during cancer therapy. IEEE Sens J 2008;8:38–50.
[11] Gurp EJB, Haanstra BKC, Murrer LHP, Van Gils FCJM, Dekker ALAJ, Mijnheer BJ, et al. In vivo dosimetry with a linear MOSFET array to evaluate the urethra dose during permanent implant brachytherapy using Iodine-125. Int J Radiat Oncol Biol Phys 2009;75:1266–72.
[12] Anderson CE, Nielsen SK, Greilich S, Helt-Hansen J, Lindegaard JC, Tanderup K. Characterization of a fiber-coupled Al2O3:C luminescence dosimetry system for online in vivo dose verification during 192Ir brachytherapy. Med Phys 2009;36:708–18.
[13] Wang LLW, Perles LA, Archambault PL, Sahoo N, Mirkovic D, Beddar S. Determination of the quenching correction factors for plastic scintillation detectors in therapeutic high-energy proton beams. Phys Med Biol 2012;57:7767–81.
[14] Jursinic PA, Yahnke CJ. In vivo dosimetry with optically stimulated luminescent dosimeters, OSLDs, compared to diodes; the effects of buildup cap thickness and fabrication material. Med Phys 2011;38:5432–40.
[15] Shin G, et al. Flexible near-field wireless optoelectronics as subdermal implants for broad applications in optogenetics. Neuron 2017;93:509–21.
[16] Piech DK, et al. A wireless millimetre-scale implantable neural stimulator with ultrasonically powered bidirectional communication. Nat Biomed Eng 2020;4:207–22.
[17] Hassler C, Boretius T, Stieglitz T. Polymers for neural implants. J Polym Sci B Polym Phys 2011;49:18–33.
[18] Shen K, Maharbiz MM. Ceramic packaging in neural implants. J Neural Eng 2021;18:025002.